Detailed description of the ENZ approach

Joseph J.M. Braat, Peter Dirksen, Sven van Haver, Augustus J.E.M. Janssen

E-mail addresses:

j.j.m.braat@tudelft.nl, peter.dirksen@philips.com, s.vanhaver@tudelft.nl and vanhaver@stcorp.nl, a.j.e.m.janssen@tue.nl

1 The diffraction integral

An aberrated optical system is described by the pupil function $P(\rho,\theta)$. Because of the circular geometry that is present in most optical problems, we switch from the real-space cartesian coordinates (X,Y,Z) (see Fig. 1) to normalized cylindrical coordinates (ρ,θ,z) with $0 \le \rho \le 1$ and $0 \le \theta \le 2\pi$. A general pupil function can be written as

$$P(\rho,\theta) = A(\rho,\theta)\exp\{i\Phi(\rho,\theta)\} \ , \tag{1}$$

where A is the (non-negative) *transmission function* and Φ is the (real) *aberration phase*. Note that for our purpose we can consider the transmission function to be a possible nonuniformity in the beam that illuminates the entrance pupil of the optical system. In the case of a mirror system with a central obstruction, the transmission function A becomes zero in a central region.

From Fourier optics, see Ref.[1], Sec. 9.1, the normalized complex point-spread function $U(r,\phi;f)$ at a defocused plane described by the defocus parameter f and polar coordinates r,ϕ with $0 \le r < \infty$ and $0 \le \phi \le 2\pi$, is given in normalized form as

$$U(r,\phi;f) = \frac{1}{\pi}\int_0^1\int_0^{2\pi} \exp\{if\rho^2\}P(\rho,\theta)\exp\{2\pi i\rho r\cos(\theta-\phi)\}\,\rho d\rho d\theta \ . \tag{2}$$

Here the factor $\exp\{if\rho^2\}$ stems from the phase departure in the exit pupil due to a focal shift by an amount of z (in units of the normalized axial coordinate). It can be shown that the relation between f and z is given by $f = -2\pi z$. The minus sign in the relationship between f and z differs from the convention used in Ref.[1] because we chose not to include a minus sign in the defocus exponential of the integrand in Eq.(2). The exponential $\exp\{2i\pi\rho r\cos(\theta-\phi)\}$ is dictated by the Huygens-Fresnel principle under the usual approximations. The issue we consider here is how to compute U from P in a numerically reliable, accurate and convenient form. For this we shall in Sec. 2 consider the Zernike expansion of P and show in Sec. 3 how this expansion translates into an analytical expression for U.

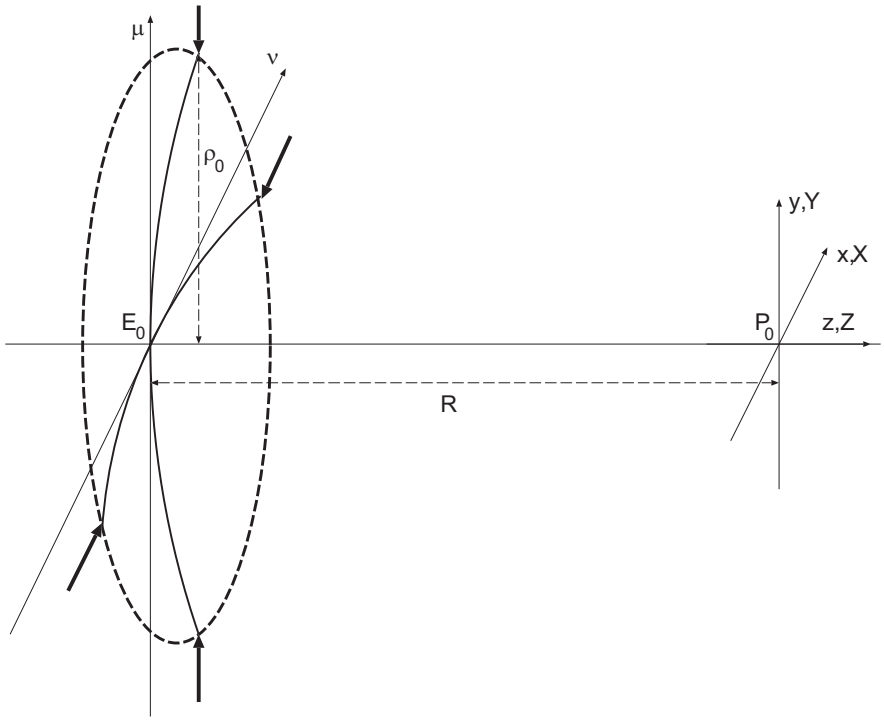

Figure 1: A wave propagates from the spherical reference surface with radius R in the exit pupil (center in E_0) towards the image plane (center at P_0). We use cylindrical coordinates instead of the cartesian set (X, Y, Z). The diameter of the exit pupil is $2\rho_0$ and the distance from pupil to image plane is R. In this document, the lateral coordinates on the exit pupil sphere are normalized to unity by means of the value of ρ_0 and denoted by (ν, μ); the corresponding normalized polar coordinates are (ρ, θ). The image plane coordinates (X, Y) are normalized with the aid of the diffraction unit, λ/s_0, and denoted by (x, y); $s_0 = \rho_0/R$ equals the image-side numerical aperture (NA) of the optical system. The corresponding polar coordinates in the image plane are (r, ϕ). The real-space axial coordinate Z is normalized with respect to the axial diffraction unit λ/u_0 with $u_0 = 1 - (1 - s_0^2)^{1/2}$, yielding $z = Zu_0/\lambda$. For optical systems with a low-to-moderate NA-value, $u_0 \approx (NA)^2/2$ and $z = (NA)^2)Z/2\lambda$.

2 Zernike representation of pupil functions

2.1 Classical viewpoint

Consider first the case that we have an optical system with only a pure-phase aberration, so that $P = \exp\{i\Phi\}$ with real Φ. Expand Φ into a *Zernike* series,

$$\Phi(\rho, \theta) = \sum_{n,m} \alpha_n^m Z_n^m(\rho, \theta) \quad , \tag{3}$$

with

$$Z_n^m(\rho,\theta) = R_n^m(\rho).\begin{cases}\cos m\theta \ , \\ \\ \sin m\theta \ .\end{cases} \tag{4}$$

$Z_n^m(\rho,\theta)$ is the Zernike circle polynomial with the radial polynomial $R_n^m(\rho)$ its radial part of *azimuthal* order m and *degree* n, with integers $n, m \geq 0$ such that $n - m \geq 0$ and even, and α_n^m is the corresponding (real) expansion coefficient. We shall consider in the sequel only the cosine option above, the sine option requiring just a second set of expansion coefficients. Another expansion is frequently used, involving complex exponentials $\exp(im\theta)$. The azimuthal order number now runs from $-\infty$ to $+\infty$ and the Zernike coefficients α_n^m are generally complex.

In the expansion of Eq.(3), the α_n^m carry physical significance, also see Ref.[1], Sec. 9.3, according to table 1 below.

Zernike terms				
$Z_0^0 = 1$	aberration-free (Z_1)		$Z_3^1 = (3\rho^3 - 2\rho)\cos\theta$	coma (Z_7)
$Z_1^1 = \rho\cos\theta$	tilt (Z_2)		$Z_2^2 = \rho^2\cos 2\theta$	astigmatism (Z_5)
$Z_2^0 = 2\rho^2 - 1$	defocus (Z_4)		$Z_4^0 = 6\rho^4 - 6\rho^2 + 1$	spherical (Z_9)

Table 1: Some characteristic lower-order Zernike terms; between parentheses the number of the Zernike polynomial is given according to the so-called fringe convention, see Ref.[2].

2.2 More general viewpoint

Consider a general pupil function $P = A\exp\{i\Phi\}$ and expand this product of functions into a Zernike series as

$$P(\rho,\theta) = A(\rho,\theta)\exp\{i\Phi(\rho,\theta)\} = \sum_{n,m}\beta_n^m Z_n^m(\rho,\theta) \ . \tag{5}$$

In the important special case that $A \approx 1$ and Φ is small, we have

$$P(\rho,\theta) \approx 1 + i\Phi(\rho,\theta) = 1 + \sum_{n,m} i\alpha_n^m Z_n^m(\rho,\theta) \ . \tag{6}$$

In the general case, the physical interpretation of the complex β_n^m may not be straightforward. There exists, however, a simple relationship between the on-axis intensity $I(0,0;0) = |U(0,0;0)|^2$ of the diffraction image and the β-coefficients: $I(0,0) = |\beta_0^0|^2$. It is also possible to establish a slightly more elaborate expression for the frequently used Strehl intensity I_S in terms of the β-coefficients after normalization with respect to the integrated intensity over the pupil:

$$I_S = \frac{|\beta_0^0|^2}{\sum_{n,m}\left(\frac{|\beta_n^m|^2}{n+1}\right)} \ . \tag{7}$$

In the case that only weak phase aberrations are present, the $|\beta_n^m|$ $(n, m \neq 0)$ are close to zero and the Strehl intensity remains unity.

The strong point of the β-representation is that only a limited number of low order β's with modest amplitude is sufficient for the accurate description of the pupil function of a high-quality optical system. Going back from the β-representation to the α's with their easier physical interpretation in the wavefront domain implies a phase 'unwrapping' procedure. Phase unwrapping may lead to 2π ambiguities, especially if the phase function is not continuous. The majority of high-quality optical systems consists of well-corrected systems with relatively small β-values and the phase-unwrapping problem is easily solved.

3 From pupil function P to point-spread function U

3.1 Analytic solution

We insert the Zernike series representation of Sec. 2.2 for P into the diffraction integral and get for the point-spread function U the expression

$$U(r, \phi; f) = \sum_{n,m} \beta_n^m U_n^m(r, \phi; f) \ , \tag{8}$$

where $\beta_n^m U_n^m$ is the contribution to U of the aberration term $\beta_n^m Z_n^m$. In [J1] it has been shown how to evaluate the U_n^m. There holds

$$U_n^m(r, \phi; f) = 2i^m V_n^m(r, f) \cos m\phi \ , \tag{9}$$

where

$$V_n^m(r, f) = \int_0^1 \exp\{if\rho^2\} R_n^m(\rho) J_m(2\pi r\rho) \rho d\rho \ , \tag{10}$$

with J_m the Bessel function of the first kind and of order m. For V_n^m there is the power-Bessel series expansion

$$V_n^m(r, f) = \exp(if) \sum_{l=1}^{\infty} (-2if)^{l-1} \sum_{j=0}^{p} v_{lj} \frac{J_{m+l+2j}(2\pi r)}{l(2\pi r)^l} \tag{11}$$

in which $p = (n-m)/2$ and

$$v_{lj} = (-1)^p \ (m+l+2j) \binom{m+j+l-1}{l-1} \binom{j+l-1}{l-1} \binom{l-1}{p-j} \Big/ \binom{q+l+j}{l} \quad , \tag{12}$$

where $q = (n+m)/2$ and the binomial coefficients are defined for integer n, k by

$$\binom{n}{k} = \begin{cases} \frac{n!}{(n-k)!k!} & , \quad 0 \leq k \leq n \ , \\ \\ 0 & , \quad \text{otherwise} \ . \end{cases} \tag{13}$$

The series expansion in (11) can also be cast into a form that is reminiscent of Lommel's series expression for the aberration-free case, viz.

$$V_n^m(r,f) = \exp(if) \sum_{l=0}^{\infty} \left(\frac{-if}{\pi r}\right)^l \sum_{j=0}^{p} u_{lj} \frac{J_{m+l+2j+1}(2\pi r)}{2\pi r} \quad , \tag{14}$$

where

$$u_{lj} = (-1)^p \, \frac{m+l+2j+1}{q+l+j+1} \binom{m+l+j}{l} \binom{l+j}{l} \binom{l}{p-j} \Big/ \binom{q+l+j}{l} \quad . \tag{15}$$

The result of the classical Nijboer-Zernike theory,

$$V_n^m(r,0) = \int_0^1 R_n^m(\rho) J_m(2\pi\rho r) \rho d\rho = (-1)^{\frac{n-m}{2}} \frac{J_{n+1}(2\pi r)}{2\pi r} \ , \tag{16}$$

is obtained from (14) by setting $f = 0$ (so that only the term in the series with $l = 0$ and $j = p$ is non-vanishing).

3.2 Summary and features of analytic solution

Having expanded the complex pupil function P as

$$P(\rho,\theta) = \sum_{n,m} \beta_n^m R_n^m(\rho) \cos m\theta \ , \tag{17}$$

the defocused complex point-spread function U is given by

$$U(r,\phi;f) = 2 \sum_{n,m} i^m \beta_n^m V_n^m(r,f) \cos m\phi \ . \tag{18}$$

Here the basic integrals V_n^m have the power-Bessel series representation

$$V_n^m(r,f) = \exp(if) \sum_{l=1}^{\infty} (-2if)^{l-1} \sum_{j=0}^{p} v_{lj} \frac{J_{m+l+2j}(2\pi r)}{l(2\pi r)^l} \tag{19}$$

with explicitly given v_{lj}.

We briefly mention another approach to solving the general diffraction integral of Eq.(2). The integrand can be split up in monomial terms in ρ according to

$$T_n^m(r,f) = \int_0^1 \exp\left\{if\rho^2\right\} \rho^n J_m(2\pi r\rho) \rho d\rho \ . \tag{20}$$

Like the $V_n^m(r,f)$, the integrals $T_n^m(r,f)$ also allow a semi-analytic solutions. Details can be found in [J1] and [B1].

The solutions possess the following features.

i) Separation of the spatial and focal variables and the optical parameters r, ϕ, f, β_n^m.

ii) Numerical evaluation feasible for all r and all f with $|f|$ up to 25 (focal depth range approximately from -15 to 15). With $3|f|+5$ terms included in the series over l, an absolute accuracy of at least 10^{-6} in amplitude is achieved.

iii) Easy and transparent computer codes; some downloadable examples of such codes, programmed in MatLab, are made available on the webpage under the heading *Downloads*.

iv) Lommel's solution (1886) for the aberration-free case and Nijboer's solution (1942) for the aberrated case at best focus $f = 0$ occur as special cases.

4 Aberration retrieval from the through-focus intensity point-spread function

In Sec. 3 we have seen how we can compute the through-focus complex amplitude U, and therefore the through-focus intensity $I = |U|^2$, from the Zernike expansion coefficients β of the pupil function P. We now consider the *inverse* problem, where we suppose the through-focus intensity I to be given and where we want to determine the pupil function P that gives rise to these intensity distributions. This is a problem of great practical importance since in the regime of optical frequencies occurring nowadays one generally has no access to the complex amplitude U while the intensity I is relatively easy to measure.

4.1 Approach

We postulate

$$P = P_{theory} = \sum_{n,m} \beta_n^m R_n^m(\rho) \cos m\theta \ , \tag{21}$$

and we estimate the unknown β_n^m by matching the measured or given intensity $I(r, \phi; f)$ with the theoretical intensity

$$I_{theory}(r, \phi; f) = |U_{theory}(r, \phi; f)|^2 = \left| 2 \sum_{n,m} i^m \beta_n^m V_n^m(r, f) \cos m\phi \right|^2 \tag{22}$$

in the $(r, \phi; f)$-space (focal region). Since there is only a limited number of non-zero β's, this is a relatively easy task for which we give a work-out below under a "small" aberration assumption.

4.2 Work-out for small aberrations

We assume that aberrations are small. On the level of β's this means that β_0^0, the coefficient of the aberration-free term $Z_0^0 \equiv 1$, dominates the totality of all other β_n^m.

Since we work with intensities, we may also assume that $\beta_0^0 > 0$, thereby fixing an undetermined overall phase factor. Then we get

$$\begin{aligned} |U_{theory}|^2 &= \left| 2\beta_0^0 V_0^0 + 2{\sum_{n,m}}' i^m \beta_n^m V_n^m \cos m\phi \right|^2 \\ &\approx 4(\beta_0^0)^2 |V_0^0|^2 + {\sum_{n,m}}' \beta_0^0 \mathrm{Re}(\beta_n^m).8\mathrm{Re}\left[i^m V_n^m V_0^{0*} \right] \cos m\phi \\ &\quad - {\sum_{n,m}}' \beta_0^0 \mathrm{Im}(\beta_n^m).8\mathrm{Im}\left[i^m V_n^m V_0^{0*} \right] \cos m\phi \, . \end{aligned} \tag{23}$$

Here the $\approx$ refers to the fact that we have deleted small cross-terms (involving two β_n^m with $(n,m) \neq (0,0)$), and the $'$ on the summation signs means to indicate that the term with $(n,m) = (0,0)$ has been omitted. The β_n^m are found by optimizing the match between the above linearized theoretical intensity and the given or measured intensity in the focal region. Here we observe that the linearized theoretical intensity $|U_{theory}|^2$ involves the quantities $(\beta_0^0)^2$, $\beta_0^0 \mathrm{Re}(\beta_n^m)$, $\beta_0^0 \mathrm{Im}(\beta_n^m)$ in a linear way (with $\beta_0^0 > 0$), viz. as coefficients of the known and readily computable *basic functions*

$$\begin{aligned} RE_n^m(r,\phi;f) &= 8\mathrm{Re}\left[i^m V_n^m(r,f) V_0^{0*}(r,f) \right] \cos m\phi \, , \\ IM_n^m(r,\phi;f) &= 8\mathrm{Im}\left[i^m V_n^m(r,f) V_0^{0*}(r,f) \right] \cos m\phi \, . \end{aligned} \tag{24}$$

A convenient procedure results when the coefficients are chosen such that the mean squared difference between the given intensity and the linearized theoretical intensity is minimal. This works well in practice when a symmetric f-range is used and when sampling in the various image planes in the focal region is done in accordance with the polar nature of the coordinates r and ϕ. The β-representation has proven to be useful up to amplitude/phase values of typically 5 to 6 for an isolated β-coefficient. For a more general aberration pattern, the *rms* value of the phase variation over the exit pupil should not exceed 1.5 radians. The total effect of the β-coefficients on the Strehl intensity, see Eq.(7), should be such that there holds $I_S \geq 0.30$. Note that the Strehl intensity of a well-corrected optical imaging system should be at least 80%.

4.3 Features of the solution

There are the following particular features of the solution of the problem as outlined above:

i) Simple linear algebra with well-conditioned linear systems.

ii) Decoupling per azimuthal order ($\cos m\phi$!).

iii) Decoupling per real and imaginary part of β_n^m (RE_n^m and IM_n^m have opposite parity in f: symmetric f-range!).

iv) Additional "lucky breaks" in the often occurring case that we have a pure-phase aberration ($P = \exp\{i\Phi\} \approx 1 + i\Phi$). Then β_0^0=1 in the inversion scheme and all other β's are purely imaginary.

5 Advanced ENZ-theory

In the previous sections we have presented the basics of ENZ-theory for the computation of point-spread functions from pupil functions and the retrieval of aberrations from intensity point-spread functions in the focal region. When using ENZ-theory in practical situations, it may well happen that not all conditions under which the basic theory is supposed to be applied are met. We discuss in this section the extensions of the ENZ-theory that are required when we deal with

i) optical systems with high numerical aperture,

ii) (lithographic) systems with blurring in the image planes and focal stochastics,

iii) optical systems with aberrations exceeding the diffraction limit.

5.1 Optical systems with high numerical aperture (vector diffraction)

The original Extended Nijboer-Zernike diffraction analysis was limited to scalar optical fields, a good approximation for imaging systems with a numerical aperture smaller than 0.60. At larger numerical aperture, several complications are encountered that have been partly treated in the literature:

i) the vector character of the light has to be accounted for because the focal field can not be described by a single quantity. In general, if the light is linearly polarized in the x-direction at the entrance of the optical system, we will also observe a dominating x-component in the focal region. But on top of this, non-negligible field components in the y- and z-direction will be measured. The calculation of each of these components requires a special diffraction integral that is more complicated than the original scalar version.

ii) the distribution of the intensity on the exit pupil of the optical system sphere is, apart from a lateral magnification factor, not a simple one-to-one mapping of the intensity distribution on the entrance pupil. One has to specify the type of optical system to determine the exact mapping. In the frequently occurring case of imaging systems with a large image field (the so-called aplanatic optical systems), a special mapping is found that leads, with respect to the lateral pupil coordinate, to an increasing intensity towards the rim of the exit pupil. This radiometric effect is of minor importance at low aperture but needs to be incorporated in the high numerical aperture case.

iii) the defocusing of a high-NA pencil of light is not simply described by multiplying the various integrands of the diffraction integrals with a quadratic phase factor. The phase departure of a defocused beam is proportional to the perpendicular pathlength difference between two spherical caps. Apart from the leading quadratic term, higher order terms need to be incorporated in the expression for the defocus effect.

iv) the vectorial diffraction integrals that were given in the literature did not allow an analytic treatment with respect to separate Zernike aberration terms. It has turned out to be possible to develop semi-analytic expressions for the basic vectorial diffraction integrals for each Zernike aberration term like it was demonstrated earlier for the scalar diffraction case. With the foregoing extensions to the scalar case we have obtained analytic expressions for the electric and magnetic field components in the focal region of a high-NA imaging system ([J4]).

The next step was to create a backward calculation scheme for the vectorial case so that the aberrations and transmission defects of a high NA optical system can be retrieved. Although the scheme, including the retrieval of the so-called 'polarisation aberration', comprises rather lengthy expressions, the retrieval at high numerical aperture has become feasible (see [J7]) and is currently applied both to synthetic data for testing purposes and to experimental data; in the latter case, only illumination with natural light was used and this leads to a rather drastically reduced version of our retrieval scheme.

We now list some of the changes and extensions that occurred in the formulae when switching from the scalar case to the high-NA case, including the introduction of the vector diffraction formalism. In the case of optical systems with a numerical aperture exceeding 0.60, the focal factor $\exp[if\rho^2]$ in the diffraction integral (2) fails to be an accurate approximation of the true focal factor $A_R(\rho)\exp[i\Phi_c(\rho)]$ in which

$$A_R(\rho) = (1 - NA^2\rho^2)^{-\frac{1}{4}} \ , \ \Phi_c(\rho) = f\frac{1 - (1 - NA^2\rho^2)^{\frac{1}{2}}}{1 - (1 - NA^2)^{\frac{1}{2}}} \ . \tag{25}$$

In (25), A_R is an amplitude function accounting for the radiometric effect and Φ_c is the phase function that correctly describes defocusing in the exit pupil. In [J6], Sec. 5, it is shown how the ENZ-theory can be simply extended to give adequate forward computation and retrieval results in the regime $0.60 \leq NA \leq 0.80$. For values of NA in excess of 0.80, this extension is not adequate anymore; moreover one has to adopt a vectorial treatment of the imaging and also the state of polarization of the used light should be taken into account. We consider, for the case of $NA \geq 0.80$, the complex pupil function on the exit pupil, according to

$$B^x = A^x \exp[2\pi i W^x] \ , \ B^y = A^y \exp[2\pi i W^y] \ , \tag{26}$$

with A^x and A^y the field strenghts in the x and y directions and W^x and W^y the wavefront aberrations in units of λ, the wavelenght of the polarized light. These B^x and B^y are expanded in series involving the Zernike terms $\exp[im\theta]R_n^{|m|}(\rho)$ with coefficients $\beta_{n,x}^m$ and $\beta_{n,y}^m$, where we adopt now, for notational convenience, the exponential rather than the trigonometric notation for the θ-dependence. A further advantage is the simultaneous treatment of amplitude and phase using the complex notation. This allows for the incorporation of birefringence that effects both the amplitude and the phase of the propagating light waves. The vector corresponding to the field arising

from an initially linearly x-polarized incident wave is given by

$$\mathbf{E}^x(r,\phi,f) = -i\gamma s_0^2 \exp\left[\frac{-if}{u_0}\right] \sum_{n,m} i^m \beta_{n,x}^m \exp\left[im\phi\right] \times \begin{pmatrix} V_{n,0}^m + \frac{s_0^2}{2} V_{n,2}^m \exp\left[2i\phi\right] + \frac{s_0^2}{2} V_{n,-2}^m \exp\left[-2i\phi\right] \\ -\frac{is_0^2}{2} V_{n,2}^m \exp\left[2i\phi\right] + \frac{is_0^2}{2} V_{n,-2}^m \exp\left[-2i\phi\right] \\ -is_0 V_{n,1}^m \exp\left[i\phi\right] + is_0 V_{n,-1}^m \exp\left[-i\phi\right] \end{pmatrix} . \quad (27)$$

Here we have written

$$s_0 = NA = \sin\alpha \ , \ u_0 = 1 - \sqrt{1-s_0^2} \ , \ f = -2\pi u_0 \frac{Z}{\lambda} = -2\pi z \ , \quad (28)$$

with α the aperture angle of the system and z the axial coordinate in units of λ. A similar expression results for the case of an initially y-polarized incident wave. For full details, see [J4], [J7]. The $V_{n,j}^m$ functions occurring in (27) are given as

$$V_{n,j}^m = \int_0^1 \frac{\rho^{|j|}\left(1+\sqrt{1-s_0^2\rho^2}\right)^{-|j|+1}}{(1-s_0^2\rho^2)^{1/4}} \exp\left[\frac{if}{u_0}\left(1-\sqrt{1-s_0^2\rho^2}\right)\right] \times R_n^{|m|}(\rho) J_{m+j}(2\pi r\rho)\rho d\rho \ . \quad (29)$$

The computation of the $V_{n,j}^m$ has been described in [J4], Appendix B, see also Subsec. 5.4 below; in [J4], Sec. 5, a number of figures, showing moduli of field components computed according to (27-29) under a variety of polarization conditions are presented. In [J7], the above forward computation scheme is taken as a point of departure to devise a retrieval method for both aberrations and birefringence for which a detailed and instrumental graphical illustration of the arising basic functions is presented. In [C4], [P10] the results of forward calculation using the vectorial high-NA formulas and those using the low-NA formulas are compared for the case of unpolarized light. Moreover, for this unpolarized case, aberration retrieval under high-NA conditions is performed.

5.2 Image blur and focal stochastics

In the lithographic application of aberration retrieval according to the ENZ-method, the recorded intensities $I'(r,\phi;f)$ are quite often a smeared version of the actual intensities $I(r,\phi;f)$. Common reasons for this smearing are

i) mechanical noise in the horizontal planes,

ii) acid diffusion in the image planes during the post exposure baking process (resist-based recording),

iii) stochastic variation of the focal parameter f.

It is customary to model the combined effects of the position noise and the diffusion in the image planes with the aid of a Gaussian convolution kernel with zero mean and radial symmetry. Furthermore, the focal parameter is assumed to have Gaussian distribution around its nominal value. Accordingly, the relation between the recorded intensity I' and the actual intensity I is

$$I'(x,y;f) = \iiint I(x,y;f)d(x-x',y-y')f_n(f-f')dx'dy'df' \quad . \tag{30}$$

Here d and f_n are given by

$$d(x,y) = \frac{1}{2\pi\sigma_r^2}\exp\left(-\frac{x^2+y^2}{2\sigma_r^2}\right) \quad , \qquad real\ x,y \quad , \tag{31}$$

and

$$f_n(f) = \frac{1}{\sigma_f\sqrt{2\pi}}\exp\left(\frac{-f^2}{2\sigma_f^2}\right) \qquad , \qquad real\ f \quad , \tag{32}$$

with σ_r and σ_f the standard deviations in the spatial domain and focal range respectively. In the retrieval scheme, it is necessary to correct the basic functions RE_n^m and IM_n^m of (24) in accordance with the integral operation in (30), where we assume the blurring effect to be linear. The numerical evaluation of the integrals in (30), with $I = RE_n^m$ or IM_n^m, is a time-consuming and delicate matter, especially when σ_r and σ_f are small. In [J8] this problem is circumvented by identifying σ_r and σ_f with diffusion times t and s according to

$$\sigma_r = \sqrt{2Dt} \quad , \quad \sigma_f = \sqrt{2cs} \quad , \tag{33}$$

with D and c diffusion constants. The recorded intensity $I'(x,y;f)$ can then be considered as the result $I(x,y;f;t,s)$ of the diffusion proces after times t, s with initial intensity $I(x,y;f;0,0)$ equal to the actual intensity $I(x,y;f)$. This diffused function $I = I(x,y;f;t,s)$ satisfies the diffusion equations

$$\frac{\partial I}{\partial t} = D\left(\frac{\partial^2}{\partial x^2}+\frac{\partial^2}{\partial y^2}\right)I \quad , \quad \frac{\partial I}{\partial s} = c\frac{\partial^2 I}{\partial f^2} \quad . \tag{34}$$

The $I(x,y;f;t,s)$ can then be approximated as

$$\begin{aligned} I(x,y;f;t,s) &= I(x,y;f;0,0) + t\frac{\partial I}{\partial t}(x,y;f;0,0) + s\frac{\partial I}{\partial s}(x,y;f;0,0) \\ &+ \frac{1}{2}t^2\frac{\partial^2 I}{\partial t^2}(x,y;f;0,0) + ts\frac{\partial^2 I}{\partial t\partial s}(x,y;f;0,0) + \frac{1}{2}s^2\frac{\partial^2 I}{\partial s^2}(x,y;f;0,0) \\ &+ \quad ... \end{aligned} \tag{35}$$

in which the required partial derivatives can de evaluated in accordance with (34). In [J8], the resulting approximations have been calculated analytically for $I = RE_{n=2p}^{m=0}$,

$IM^{m=0}_{n=2p}$. We have, for instance, for $|V^0_0|^2$ the first order corrected expression (with σ_r and σ_f reinstalled according to (33))

$$\begin{aligned} |V^0_0|^2 &- \pi^2\sigma_r^2\left(2|V^0_0|^2 + 2\mathrm{Re}\left(V^0_2 V^{0*}_0\right) - 4|V^1_1|^2\right) \\ &- \frac{1}{2}\sigma_f^2\left(\frac{1}{6}|V^0_0|^2 + \frac{1}{3}\mathrm{Re}\left(V^0_4 V^{0*}_0\right) - \frac{1}{2}|V^0_2|^2\right) \quad . \end{aligned} \tag{36}$$

In Sec. 5.4 below we shall sketch a more systematic approach for evaluating Laplacians and $\frac{\partial}{\partial f}$ of basic functions.

5.3 Retrieval of larger aberrations: predictor-corrector approach

In (23) we have linearized $|U_{theory}|^2$ with respect to terms involving products $\beta^0_0\mathrm{Re}(\beta^m_n)$, $\beta^0_0\mathrm{Im}(\beta^m_n)$. This is a valid approach when the totality of all β^m_n with $(n,m) \neq (0,0)$ is relatively small compared to β^0_0. For larger aberrations it is better to adopt a predictor-corrector approach. Here a sequence $\beta^m_n(k), \quad k = 0, 1, \ \ldots$, of estimates of the β^m_n is constructed in which $\beta^m_n(0)$ is the result of the matching procedure described in Subsec. 4.2. The estimate $\beta^m_n(k{+}1)$ is obtained from $\beta^m_n(k)$ by applying the matching procedure with the recorded intensity corrected for the k^{th} estimate

$$4 \sum_{n_1,m_1;n_2,m_2}{}'' \ \mathrm{Re}\left[\beta^{m_1}_{n_1}(k)\beta^{m_2*}_{n_2}(k) i^{m_1-m_2} V^{m_1}_{n_1} V^{m_2*}_{n_2}\right] \cos m_1\varphi \cos m_2\varphi \tag{37}$$

of the small-cross-terms contribution where the $''$ at the summation sign refers to the totality of all n_1, m_1, n_2, m_2 with $(n_1, m_1) \neq (0,0) \neq (n_2, m_2)$. In [J6] this procedure has been worked out in simulation, and it was found that aberrations well exceeding the diffraction limit could be perfectly retrieved. As a rule of thumb, we proved retrieval convergence for an rms aberration value of 0.25 λ, approximately three times the diffraction limit of 0.075 λ rms.

5.4 The general integral

The general basic function, as occurs in (37), in its high NA-version, as we have it in (29), involves the product of an integral

$$\begin{aligned} J(k,j,l;E) = \quad & i^l \int_0^1 \rho^k \left(1 + \sqrt{1 - s_0^2\rho^2}\right)^{-j+1} \quad \times \\ & E(\rho) \exp\left[\frac{if}{u_0}\left(1 - \sqrt{1 - s_0^2\rho^2}\right)\right] J_l(2\pi\rho r)\rho d\rho e^{il\phi} \end{aligned} \tag{38}$$

with the complex conjugate of another such integral. Here $E(\rho)$ is a relatively smooth function of ρ, such as

$$\frac{1}{(1 - s_0^2\rho^2)^{\frac{1}{4}}} \frac{J_1(b\rho)}{\frac{1}{2}b\rho} R^m_n(\rho). \tag{39}$$

The factor $(1-s_0^2\rho^2)^{-\frac{1}{4}}$ represents the radiometric effect. The factor $J_1(b\rho)/\frac{1}{2}b\rho$ represents a second amplitude non-uniformity that occurs when the pinhole used for producing the point-spread functions has a non-negligible diameter b (normalized). The factor $R_n^m(\rho)$ is a Zernike polynomial of moderate degree n and azimuthal order m.

The integrals J transform conveniently under applying the Laplacian $\Delta = \frac{\partial^2}{\partial x^2} + \frac{\partial^2}{\partial y^2}$ or partial derivatives ∂_x, ∂_y, ∂_f. There holds

$$\Delta J(k,j,l;E) = -4\pi^2 J(k+2,j,l;E) \ , \tag{40}$$

$$\partial_x J(k,j,l;E) = \pi i J(k+1,j,l+1;E) + \pi i J(k+1,j,l-1;E) \ , \tag{41}$$

$$\partial_y J(k,j,l;E) = \pi J(k+1,j,l+1;E) - \pi J(k+1,j,l-1;E) \ , \tag{42}$$

$$\partial_f J(k,j,l;E) = \frac{is_0^2}{u_0} J(k+2,j+1,l;E) \ . \tag{43}$$

Hence, in the case of high-NA imaging with image blur and focal stochastics, the terms that occur in (35) via (34), are all expressible in terms of the general integral J. In [J4], Appendix B, a method has been given to evaluate integrals J, but this method is relatively complicated. We have devised a more user-friendly computation scheme that can be used when the degree n of the Zernike polynomial R_n^m involved in E is not too large, see [B1], Appendix D and [J18].

5.5 Imaging of extended objects

A new field of application can be found in the forward calculation of more complicated object structures as encountered in optical lithography. The aerial image or, more importantly, the resist image with an as large as possible tolerance against image plane and exposure off-set (critical dimension or 'CD'-control in lithography) has to be determined by finding an optimum diffracting structure on the mask or reticle in the object plane of the projection lens. To this end, on top of the basic geometrical features, extra amplitude and/or phase structures are introduced and iteratively adjusted on the object mask. This optimization method, called **O**ptical **P**roximity **C**orrection (OPC), is largely based on an electromagentic solver for computing the optical near-field of the mask for each angle of incidence coming out of the illumination system, on the Fast Fourier Transform (FFT) for propagation of the coherent optical field towards the entrance pupil of the projection system and on singular value decomposition (SVD) for computing the partially coherent image formation. The total numerical load of such a mask optimization by means of OPC is impressive and asks for a large installation of computing power. In the case of vector diffraction, Hopkins' approximation of the diffraction by a grating (invariance with respect to the angle of incidence) is not allowed and this leads to a further numerical complication that severely slows down the OPC-optimisation process.

To be adopted for OPC-calculations, ENZ-theory has to be generalised with respect to the object structure. Instead of using the small 'point-source' with an extension of typically less than, say, $\lambda^2/4(NA)^2$, that was the starting point in the ENZ-theory, we now switch to extended objects that are not necessarily illuminated in a coherent way.

In the ENZ-approach for mask imaging, the near-field calculation remains subjected to an electromagnetic field solver. But in the other imaging steps, ENZ-theory replaces the FFT- and SVD-operations and provides a through-focus aerial image in a single step. This can equally well be done in the case of a slightly aberrated projection system. To this end, the following steps have to be executed,

- propagate the optical near-field from a finite object area (typically 100 to 1000 surface units of $\lambda^2/(NA)^2$) towards the entrance pupil using a typical angle of incidence from within the illumination cone,
- calculate the Zernike field representation in the entrance pupil of the coherent field belonging to the particular angle of incidence in the illumination,
- propagate the field from the entrance to the exit pupil of the projection system by multiplying the field in the entrance pupil with the Zernike coefficients of the non-ideal projection system; a new set of Zernike coefficients in the exit pupil is available; here, we have to include the finite magnification effect ($M \neq 0$) on the calculation of the amplitude factor $1/(1-s_0^2\rho^2)^{-1/4}$ in the integrand of the Debye integral, see Eq.(29). This factor, in the case of an object at infinity, is composed of a pupil mapping factor $\sqrt{k_z}$ multiplied by the Debye weighting factor $1/k_z$ for a plane wave, leading to the net effect of $1/\sqrt{k_z} = 1/(1-s_0^2\rho^2)^{1/4}$. In the case of a finite magnification M, the pupil mapping effect leads to an modified amplitude on the exit pupil equal to $(1-s_0^2\rho^2)^{1/4}/\{1-(n_1^2/n_0^2)M^2s_0^2\rho^2\}^{1/4}$, where we accommodated the effect of the possibly different refractive indices of object and image space, n_0 and n_1, respectively, through the ratio n_1/n_0. Including the $1/k_z$-factor, proper to the Debye-integral, we obtain the modified expression for the $V_{n,j}^m$-function of Eq.(29) for the case of finite magnification M,

$$V_{n,j}^m = \int_0^1 \frac{\rho^{|j|}\left(1+\sqrt{1-s_0^2\rho^2}\right)^{-|j|+1}}{(1-s_0^2\rho^2)^{1/4}(1-(n_1^2/n_0^2)M^2s_0^2\rho^2)^{1/4}} \exp\left[\frac{if}{u_0}\left(1-\sqrt{1-s_0^2\rho^2}\right)\right] \times R_n^{|m|}(\rho)J_{m+j}(2\pi r\rho)\rho d\rho \ . \quad (44)$$

- calculate the intensity distribution in the focal volume using the scalar or vector version of the Extended Nijboer-Zernike theory.
- Repeat the foregoing steps for other angles of incidence so that the total illumination cone is sampled in a sufficiently accurate way.
- The total energy density in the focal volume equals the incoherent sum of all partial contributions from the complete illumination cone.

An analytic tool like the ENZ-theory can be of great value because of its basic inherent accuracy, quick convergence and analytic decomposition of the focal intensity distribution along the three axis of the cylindrical coordinate system. Moreover, aberrations are readily included in the modeling and the through-focus exposure is immediately available.

5.6 Imaging in a stratified medium

Imaging in a layered or stratified medium frequently occurs, for instance, in microscopy and in optical projection lithography. The ENZ-based imaging method uses the Debye integral as its starting point, both for low to moderate and for high-NA imaging. The amplitude and phase of the spectrum of plane waves that propagate from the exit pupil to the image region determine the Zernike expansion of this wave field. The plane wave spectrum can be monitored when it is incident on a planar interface between two media, preferably perpendicular to the optical axis. A reflected and a transmitted plane wave spectrum can be calculated using standard expressions for the Fresnel reflection and transmission coefficients at an interface. For a sequence of transitions, stable schemes are available to obtain the forward and backward propagating wave amplitudes in any layer of the stratified medium. In practice by using a sufficiently large number of propagation directions to represent the full angular spectrum, we obtain, by interpolation, a smooth representation of the forward and backward propagating spectra. These spectra are then expanded with the aid of two sets of complex Zernike coefficients. In the vector case, four sets of Zernike coefficients are needed. The complete calculation scheme can be found [J18]. Research is going on to deal with surface waves and plasmonic effects in the multilayer stack. Evanescent waves that tunnel through a low-index interstice in a multilayer stack also need a special treatment that has not yet been evaluated.

5.7 Microlenses

Microlenses have many applications. In the framework of illumination optics, they are used in image sensors and in depth simulating optical arrangements. In metrology, they are used for wavefront tilt and wavefront curvature sensing, for instance in a Shack-Hartmann wavefront sensor. In such applications, the through-focus intensity distribution is needed. The Debye integral is not an adequate approximation of the field in focus when the Fresnel number of the focusing beam becomes small. The Fresnel number of a focusing beam is defined by the number of Fresnel zones that fit in the planar aperture, as seen from the focal point. For an aperture diameter of $2a$ and an image distance l, we have

$$N_F = \frac{a^2}{l\lambda} \ , \tag{45}$$

with N_F the Fresnel number and λ the wavelength of the light in the image space.

Pioneering work on this subject was carried out by Wolf and Li[3]. In Ref. [B1], Fig.(2.5), some numerical examples are shown where the Debye integral turns out to yield a bad approximation of the physical problem at hand and the Rayleigh diffraction integral should be used instead. It has turned out that the Rayleigh integral can be adapted to the ENZ-framework by applying some relatively simple scaling rules to the focal distribution according to the Debye integral. Denoting the coordinate choice and the calculation result according to the Debye integral by the index D, the field amplitude and scaled coordinates according to the Rayleigh diffraction integral are

found by the transformations

$$A_{0,R} = \frac{l}{l+z_D} A_{0,D} \ , \qquad z_R = \frac{l}{l+z_D} z_D \ , \qquad r_R = \frac{l}{l+z_D} r_D \ , \tag{46}$$

with z_D the defocusing, $A_{0,R}$ the on-axis amplitude following from the Rayleigh integral and z_R and r_R the axial and transverse coordinates to be used in the Rayleigh end result, the calculations having been carried out at coordinates z_D and r_D with the aid of the Debye integral, see also [P27].

5.8 Pupil scaling and decentring

In various diffraction problems in optics the size or shape of the diaphragm is not fixed. A well-known example of such a variable diaphragm is the iris of the eye. But also in astronomical observation special pupil configuration are encountered, for instance, the central obstruction of a telescope and a special pupil map of an aperture synthesis system. In optical lithography, a smaller diaphragm size is sometimes used to facilitate the printing of certain features. Modified Zernike polynomials that are orthogonal on an annular pupil have been devised by Mahajan[4], with the obscuration factor ϵ of the central obstruction as a parameter. The more general problem of finding the Zernike expansion of a scaled pupil from the expansion coefficients of the nominal pupil function has been solved in an elegant way in [J10]; applications of these new scaling formulae are found in [J15]. For the more general subject of finding the Zernike expansion of a scaled and shifted pupil, see also Sect. 7.4 and [J19].

5.9 Energy and momentum transport in the focal region

The availability of semi-analytic expressions for the electric and magnetic field components in a high-numerical-aperture focused field enable the analysis of EM-quantities like the electric and magnetic energy density, the Poynting vector, the vector components of the linear and angular momentum density and their three-dimensional flow components. Ref. [D1] presents the conservation laws of these quadratic EM-quantities in a high-NA focal field. In Ref. [J14] explicit expressions are given for the electromagnetic quadratic quantities in terms of the ENZ-based through-focus field components. The analysis enables the separation of orbital and spin-induced angular momentum in the focal region of a general incident beam in the entrance pupil with an elliptical state of polarisation.

6 Survey of literature and applications of ENZ theory

The ENZ-theory started with [J1] in which the power-Bessel series of the Lommel type for the diffraction integral involving a general aberration term Z_n^m is presented. This paper [J1] was followed immediately by [J2] where the solution of the forward problem was treated (calculation of the through-focus point-spread function from the pupil function using its Zernike expansion). In [J2] the merits of the new approach for

forward calculations are established from an optical point of view and a rule-of-thumb is developed for the number of terms one should include in the infinite power-Bessel series (normally $3|f| + 5$ suffices). The extension of the forward calculation to more complicated object structures is considered and the influence of the illumination coherence is included for a simple two-point resolution test.

In [J5] a different series expansion for the basic general diffraction integral is presented. These alternative expansions involve products of two types of Bessel functions and arise when Bauer's formula expressing $\exp\{if\rho^2\}$ as an infinite series involving products of spherical Bessel functions $j_k(f/2)$ and Zernike polynomials $R^0_{2k}(\rho)$ of order $m = 0$, is used in conjunction with relatively new results from the theory of orthogonal polynomials. In particular, the important problem, see Ref.[1], pp. 534-535, of systematically writing the product of two Zernike polynomials of order m_1, m_2 as a linear combination of Zernike polynomials of order $m_1 + m_2$ can be solved with these recent results. The resulting Bessel-Bessel series representation generalizes a result of the "classical" Nijboer-Zernike theory for the aberration-free case $m = n = 0$. Bessel-Bessel series representations are somewhat more complicated than the representations of the Lommel type, but have the advantage that they are practically immune to loss of digits, irrespective how large f and/or r are.

In [J4] the Zernike-based solution for the forward problem is extended to cover the case of aberrated, high-aperture optical systems. In this extension, the focal factor $\exp\{if\rho^2\}$ is replaced by its correct version $\exp\{(if/u_0)[1 - (1 - s_0^2\rho^2)^{1/2}]\}$ with $u_0 = 1 - (1 - s_0^2)^{1/2}$ and $s_0 = NA$, the numerical aperture of the system. Furthermore, the radiometric effect, manifesting itself by a factor $(1 - s_0^2\rho^2)^{-1/4}$ by which the pupil function must be multiplied, is accounted for. Moreover, in [J4], the vector character of the electromagnetic field is taken into account, including the state of polarization of the light used. In [J4], the squared modulus of the field is displayed as well as the spatial distribution of the Poynting vector in the focal region. These results were also presented in part at two scientific meeting, see [P2], [P4].

A further extension of the forward calculation method applies to the imaging of extended objects. The object is illuminated with a coherent beam of light, preferably a plane wave from a specified direction. The diffracted field on the entrance pupil sphere is calculated, using a scalar or vector diffraction method. The propagation of the complex field on the entrance pupil sphere is propagated towards the exit pupil, including the amplitude and transmission function of the optical system. The Zernike expansion of the field in the entrance pupil is multiplied by the complex lens function, in terms of its Zernike expansion. With the resulting field on the exit pupil sphere, expressed by means of a set of Zernike coefficients, we obtain the field in the focal region using the customary ENZ method. The main difference with the standard propagation method is the more complicated initial field on the entrance pupil. Normally, a very limited number of lower order Zernike coefficients are required to describe the entrance pupil field. In the presence of a complicated object, the diffracted field on the entrance pupil sphere needs Zernike coefficients of very high order, both radially and azimuthally. Typical maximum order numbers are 20, in extreme cases up to 30 or 40. More complicated illumination patterns, ranging from partially coherent to fully inco-

herent, are simulated by summing a larger number of mutually incoherent plane waves form various directions that represent with sufficient accuracy the incident illumination intensity. The complete scheme for the imaging of an extended object is found in [J17]. A comprehensive description is also found in [D2].

Point-source and extended imaging in a piecewise inhomogeneous image space frequently occur in optical imaging. When the medium is stratified, with a sequence of parallel interfaces separating media with different refractive index, the ENZ-method can be used provided the interfaces are perpendicular to the optical axis. The forward and backward propagating fields in each layer can be calculated using the standard approach for plane wave propagation in such a layered medium (matrix method, scattering matrix method, optical admittance method etc.) The forward and backward components each produce their coherent focal field distributions. Because these fields have been derived from the same coherent source point, interference effects arise. The coherent interference effects give rise to, for instance, standing wave patterns. The calculation procedure for imaging in a stack of thin layers has been described in [J17] and [D2].

The papers [J1], [J2] on the solution of the forward problem were soon followed by a contribution at the SPIE Microlithography 2002 conference [C1] on the solution of the inverse problem of aberration retrieval; an extended version of [C1] is the journal paper [J3]. In [C1] and [J3] the proof-of-principle of the aberration retrieval method is given for the case of small pure-phase aberrations in a practical lithographic setting. Also, there is briefly hinted at the method for retrieval of general aberrations. The various "lucky breaks" that occur for the pure-phase version, such as immunity to deletion of small cross-terms in the theoretical intensity and only third-order errors due to linearizing $\exp\{i\Phi\}$ as $1 + i\Phi$, were noted in [C1], [J3]. Furthermore, the forward and backward solutions are corrected for the realistic situation that the pinhole that is being imaged has a finite size (instead of being a true delta function). This is simply done by replacing the (real) focus value f in $\exp\{if\rho^2\}$ by a complex value $f + id$, where d is directly related to the diameter of the pinhole. A basic survey of the ENZ-approach, both for the forward problem and the inverse problem, with some emphasis on applications in a lithographic context, is presented in [C5]. Further validations of the aberration retrieval method are given in [C2] where experimental results, achieved on a modern wafer scanner, are shown. In particular, [C2] contains pictures that show retrieval results for aberrated lithographic lenses to which specific pure-phase aberrations of known size were intentionally added.

A further extension of the retrieval methodology in lithography is the inclusion of the effects of spatial diffusion and of focal statistics. This requires appropriate modification of the basic functions RE_n^m, IM_n^m in the retrieval equations. Some details for this are given in [C3], where diffusion parameters and focal variances are estimated along with spherical aberration coefficients. An extended and considerably more detailed version of [C3] is [J8]. In the latter manuscript, the correction of the basic functions corresponding to radially symmetric aberrations is done analytically to second order for the leading basic function involving $|V_0^0|^2$ and to first order for the basic functions involving the $V_{2p}^0 V_0^{0*}$ with $p = 1, 2, ..$, see (24). This avoids the numerical evaluation

of the required convolution integrals which is a time-consuming and delicate matter, especially when the diffusion parameters and focal variances are small. In addition, in [C6] we discuss the application of ENZ to aerial image based lens metrology and lens adjustment, the experimental results pertaining to a prototype DUV lens ($NA = 0.75$, $\lambda = 248$ nm). In this application, the ENZ-method has been adjusted for chromatic errors in accordance with the corrections discussed above. There is good agreement with results obtained from an interferometric experiment, where the ENZ-method has the advantage that both phase AND transmission errors are estimated.

The aberration retrieval methods have also been validated by performing extensive simulations in [J6]. Here the "lucky breaks" that occur for the pure-phase retrieval method are explained and illustrated by consideration of special aberrations $1+i\alpha_n^m Z_n^m$, $\exp\{i\alpha_n^m Z_n^m\}$. These "lucky breaks" do not occur, however, for the case of generally aberrated pupil functions. For the latter case, an iterative version of the method is proposed in which in each iteration step the deleted small cross-terms are estimated and included in the procedure by feeding back the β's from the previous step. It is observed in [J6] that then perfect reconstruction occurs for aberrations that may well exceed the diffraction limit. Furthermore, a simple but effective procedure is developed in [J6] to account in the diffraction integral for effects like the use of pinholes of finite size and the radiometric effect.

An extension of the general aberration retrieval method has been presented in [J7] where the high-NA effects have been included in accordance with the vector diffraction theory. Although the formulae that describe the through-focus intensity have a quite complicated nature, it is again possible to extract the harmonic azimuthal functions in the theoretical expression for the intensity in the focal region. Not only the geometrical aberration and transmission errors of the optical system but also the birefringence effects are of importance now. By collecting the data from four through-focus intensity maps, it is, in principle, possible to retrieve the complete 'polarization' aberrations of a high-NA optical system. Like in the scalar diffraction case, it is possible to establish an equation for the vector diffraction case in which the measured through-focus intensity distribution is approximated by a linearized analytic expression for the intensity containing the unknown Zernike coefficients (see master thesis [T1] and [J9]). The incident light can have arbitrary polarization; successive intensity measurements with orthogonal linear and/or circular polarization states allow the retrieval of the polarization aberrations of the system. An iterative scheme has also been applied in the vector diffraction case and it was demonstrated that Zernike coefficients converge to a final stable value once they are bound to an interval of typically one wavelength or 2π in the phase domain. As a special case, we discuss in [C4] (and [J8]) the extension of aberration retrieval to high-NA optical systems if the pin-hole source is illuminated with unpolarized light and the aberrations are restricted to be circularly symmetric. A simplified version of the vector diffraction analysis can be used here and it has been applied to experimental data pertaining to an immersion scanner (NA=0.85, λ=193 nm).

Various presentations on the aberration retrieval methods were given at scientific meetings, see [P1], [P3], [P5], [P6], [P7], [P8], [P9,abstract], [P9,poster], [P10], [P11],

[P12], [P13], [P14], [P29]. The more general references for aberration retrieval are [B1] and [D2].

7 Some related results and developments

In the process of establishing the ENZ-theory, we have obtained several results of mathematical nature on Zernike polynomials and aberrated optical systems that are also interesting outside the context of ENZ. These results have been published only in part and include

1. An extensive list of explicit Zernike expansions of functions given in analytic form.
2. Explicit results on Zernike expansion coefficients and Strehl ratios for pupils with reduced apertures.
3. Strehl ratio approximation for high-numerical-aperture systems.
4. DFT-algorithm for the computation of Zernike polynomials of arbitrary high degree n and azimuthal order m and various related results.

1. The list mentioned in 1 contains the Zernike expansions of

   a. Radial functions with Zernike^m-expansions of the form $\sum_{j=0}^{\infty} \beta_{m+2j}^m R_{m+2j}^m$ such as

   $$\rho^\alpha \ (\mathrm{Re}\,(\alpha) > -m-2) \ , \ J_k(b\rho) \ (m=k) \ , \ 1-\sqrt{1-s_0^2\rho^2} \ (m=2) \ , \qquad (47)$$

   and the Zernike^0-expansions for the functions

   $$(1-s_0^2\rho^2)^\alpha \ , \ \ln\left(1\pm\sqrt{1-s_0^2\rho^2}\right) \ , \ e^{\alpha\rho^2} \ , \ \frac{J_1(b\rho)}{b\rho} \ , \ \cdots \ . \qquad (48)$$

   b. Pure phase aberrations $\exp[i\alpha Z(\rho,\theta)]$ with $Z(\rho,\theta)$ any of the primary aberrations as listed in Table 1 on p. 3. One such expansion occurs in the paper JOSA-A, Vol. 22 (2005), 2569-2577, where it is used for an application in digital holography using an elliptical, astigmatic Gaussian beam.

   c. Explicit and closed form Zernike expansions of $\rho^k R_n^m(\rho)$, $\rho^{-l} R_n^m(\rho)$, and of the indefinite integral $\int \rho^k R_n^m(\rho) d\rho$. One such result is

   $$\rho^k R_n^m(\rho) \ = \ \sum_{j=0}^{k} \frac{n+k-2j+1}{n+k-j+1} \frac{\binom{p}{j}\binom{q+k-j}{q}}{\binom{n+k-j}{k}} R_{n+k-2j}^{m+k} \ , \qquad (49)$$

   where $p=(n+m)/2$, $q=(n-m)/2$ and $k=0,1,\cdots$. In these expansions, the upper index of the Zernike polynomials is independent of the summation index, but we have also results where the lower index is constant, see [J18], [D2].

2. Assume that we have a pupil in its Zernike representation

$$P(\rho,\theta)=\sum_{n,m}\beta_n^m R_n^m(\rho)\cos m\theta \quad ,\ 0\le\rho\le 1,\ \ 0\le\theta\le 2\pi\ , \tag{50}$$

and consider for $\varepsilon\in(0,1)$ the "scaled" pupil

$$P(\varepsilon\rho,\theta) \quad ,\ 0\le\rho\le 1,\ \ 0\le\theta\le 2\pi\ . \tag{51}$$

Then the scaled pupil function has Zernike expansion

$$P(\varepsilon\rho,\theta)=\sum_{n,m}\beta_n^m(\varepsilon) R_n^m(\rho)\cos m\theta \quad ,\ 0\le\rho\le 1,\ \ 0\le\theta\le 2\pi\ , \tag{52}$$

in which the $\beta_n^m(\varepsilon)$ can be computed from the full-scale pupil coefficients β_n^m according to

$$\beta_n^m(\varepsilon)=\sum_{n'=n,n+2,\cdots}\beta_{n'}^m\left[R_{n'}^n(\varepsilon)-R_{n'}^{n+2}(\varepsilon)\right], \quad n=m,m+2,\cdots\ . \tag{53}$$

This result, with some of its consequences in a lithographic context, appears in [J10]. A further elaboration, with special attention to Strehl ratios of scaled pupils and aberration retrieval on scaled and annular pupils, is given in [J15], see also [P15].

3. In [J11] we consider the Strehl ratio and optimum focus setting for the case of optical systems with a high NA. It turns out that both the approximating expression for the Strehl ratio and the value of the optimal focus setting (maximizing the Strehl ratio) significantly deviate from the low-NA expression and value from $NA=0.90$ onwards. This deviation stems largely from the fact that the commonly used quadratic approximation of the defocus part becomes inadequate at high NA. We develop very accurate and feasible approximations to both the Strehl ratio and the optimal focus setting in [J11] and illustrate these for the case of spherical aberration and astigmatism with $NA=0.95$.

4. In [J13] a new formula for Zernike polynomials is developed,

$$R_n^m(\rho)=\frac{1}{N}\sum_{k=0}^{N-1}U_n(\rho\cos\frac{2\pi k}{N})\ \cos\frac{2\pi mk}{N} \quad ,\ 0\le\rho\le 1\ , \tag{54}$$

where N is any integer $>n+m$, and U_n is the Chebyshev polynomial of the second kind and of degree n. The evaluation of $R_n^m(\rho)$ in the representation (54) is feasible no matter how large m and n are (the commonly used polynomial representation $R_n^m(\rho)=\sum_{s=0}^{p}(-1)^s\binom{n-s}{p}\binom{p}{s}\rho^{n-2s}$ is not feasible for large n and m due to the binomials). Moreover, by using the Fast Fourier Transform, one can produce the values of all Zernike polynomials $R_n^m(\rho)$ (with $m\le n$) at a particular point $\rho\in(0,1)$ in $O(N\log N)$ operations. The representation (54) follows from the (error-free) discretization of the formula

$$R_n^m(\rho)=\frac{1}{2\pi}\int_0^{2\pi}U_n(\rho\cos\theta)\cos m\theta d\theta \quad ,\ 0\le\rho\le 1\ , \tag{55}$$

that is proved in [J13] using Radon Transform formulas for Zernike polynomials. The representation (55) is also a very good starting point to obtain the asymptotic behaviour of the $R_n^m(\rho)$ as m and $n \to \infty$. For instance, one obtains by a straightforward application of the stationary-phase method to the integral in (55) the approximation

$$R_n^m(\rho) = 0 \quad , \, 0 \leq \rho \leq u - \varepsilon \, , \tag{56}$$

$$R_n^m(\rho) = \frac{2 \sin \left[(n+1)F - mG + \frac{1}{4}\pi \right]}{((1-\rho^2)(\rho^2-u^2))^{\frac{1}{4}} \sqrt{2\pi(n+1)}} \quad , \, u + \varepsilon \leq \rho \leq 1 - \varepsilon \, , \tag{57}$$

where

$$u = \frac{m}{n+1} \, , \quad F = \arccos \left(\frac{\rho^2 - u^2}{1 - u^2} \right)^{\frac{1}{2}} \, , \quad G = \arccos \frac{1}{\rho} \left(\frac{\rho^2 - u^2}{1 - u^2} \right)^{\frac{1}{2}} \, , \tag{58}$$

as $n, m \to \infty$ and u is bounded away from 0 and 1. Also, for the cases that ρ is near 0, u or 1, one can obtain with somewhat more effort useful results from (55).

A further striking result that is associated with the ones just given is the following one. Assume that we have a pupil function $P(\rho, \theta) \equiv p(\nu, \mu)$ that depends on one variable, say ν, only. Thus we have that

$$P(\rho, \theta) = f(\rho \cos \theta) = f(\nu) \, , \quad -1 \leq \nu \leq 1 \, , \tag{59}$$

for some function $f(\nu)$. Then the Zernike expansion of P is given as

$$P(\rho, \theta) = \sum_{m=0}^{\infty} \sum_{n=m,m+2,\cdots} \varepsilon_m (t_n - t_{n+2}) R_n^m(\rho) \cos m\theta \, , \tag{60}$$

where $\varepsilon_m = 1$ for $m = 0$ and $\varepsilon_m = 2$ for $m = 1, 2, \cdots$ (Neumann's symbol), and t_n are the Fourier cosine series expansion coefficients of $f(\cos x)$,

$$f(\cos x) = t_0 + 2 \sum_{n=1}^{\infty} t_n \cos nx \, . \tag{61}$$

5. Recently, a number of new analytic results for the Zernike polynomials were established using the basic result of Eq.(16) from the classical Nijboer-Zernike theory, see [J19]. Thus there are given explicit formulae for

(a) the expansion coefficients of scaled-and-shifted circle polynomials (compare 7.2 where only scaling was considered),
(b) the expansion coefficients of the correlation of two circle polynomials,
(c) the Fourier coefficients occurring in the cosine representation of the radial polynomials.

The result in (a) has applications in both optical lithography and ophthalmology. The result in (b) is of great interest when calculating transfer functions in optical imaging from the Zernike expansion of the pupil function that gives rise to the transfer function as an autocorrelation function. The result in (c) is of importance when the pupil disk is sampled according to a separable sampling scheme $\rho_k \exp(i\theta_l)$ in which $\rho_k = \cos\{\pi(k - 1/2)/2K\}$ with $k = 1, \cdots, K$; see [P18] for the merits of such a scheme.

8 Current and future research

Several long-term ENZ research options are pursued at this moment.

i) **High-NA aberration retrieval**

In the beginning, the retrieval operations have been limited to the scalar diffraction case; the method now has to be extended to the case of high-NA optical systems. The forward problem for the high-NA case is already considerably more complicated than the low-NA forward problem, and this is reflected in the inverse problem by a corresponding increase in complexity, see [J7]. The first results of high-NA retrieval have been obtained with 'synthetic data'. With this expression we mean that analytically obtained intensity data in the focal volume (ENZ forward calculation) have been used to replace the measured data that eventually are needed to go back to the aberrations and transmission defects of an optical system. The next step is to use measured intensity data that have been obtained for a variety of incident states of polarization. In this way we can go back not only to geometrical aberrations of the optical system but also to its birefringence properties ('polarization aberrations'). However, for the case that the illuminating light may be assumed to be unpolarized (which, up to now, is a realistic assumption in the lithographic practice) and the aberrations may be assumed to be radially symmetric, a simplification occurs so that the resulting retrieval scheme strongly resembles the scheme that was found for the low-NA systems. These developments are described in [J7], [C4]. A further enhancement of the general retrieval method consists of incorporating and using the iterative option of the general method. This option has been applied to the high-NA case with synthetic data and leads to exact solutions after a modest number of iterations (typically 5 to 10). The application of the iterative procedure to an experimental set-up as encountered in lithographic applications is the logical next step. Aberration retrieval of optical systems with special pupil shapes, for instance a central obstruction, is also a quite straightforward extension, see [P24] and [D2].

ii) **Imaging in electron microscopy**

Further possible applications could be found in high-resolution electron microscopy operating close to the diffraction limit. Both aberration retrieval and the measurement of the far-field intensity distribution of sources could be of interest.

iii) **Aperture synthesis imaging**

The coherent behaviour of arrays of apertures could also be characterized by a Zernike expansion of the transmission function of the synthetic aperture and its composite aberration pattern, constructed from the individual apertures and their mutual wavefront piston and tilt errors. The application will necessarily be limited to relatively 'dense' aperture geometries. Very 'dilute' synthetic apertures will pose serious convergence problems with respect to the Zernike expansion.

iv) **Stochastic imaging (atmospheric perturbations)**

Imaging through turbulent media (e.g. astronomical observation through the atmosphere) has been analyzed using Zernike expansions of the stochastic wavefront function. Correction of the atmospheric turbulence using adaptive optics requires the derivation of an optical error signal that allows the mirror deformation of the adaptive optical element to counteract the atmospheric perturbation. ENZ-theory is capable of accurately analyzing the (heavily) aberrated through-focus point source images that are produced by the atmospheric perturbation. The retrieval method then produces the steering signal for the deformable optical element.

v) **Various subjects**

Pupil scaling has been studied with formulae that are easily accessible as compared to previous results from the literature. Applications are found in ophthalmology and optical lithography. As a spin-off, compact formulae have been found to incorporate the effect of pupil or sub-pupil decentering. These results are of immediate interest to the astronomical community when aperture synthesis is used as a stellar imaging technique.
ENZ-theory has also been applied in the field of acoustics where the Rayleigh diffraction integral governs the sound diffraction, see Sec. 9.
The special conditions to correctly retrieve aberrations when dealing with microlenses have been taken into account int the ENZ-theory. Experiments are going on in which the adapted ENZ-theory is tested by comparing the retrieved aberration function of a microlenses with results from an interferometric measurement.

9 Acoustic diffraction and the Nijboer-Zernike approach: ANZ

9.1 Introduction

In acoustic radiation, the solution of the Helmholtz equation for the radiated pressure in the field assumes a form that is tractable for computation in two important cases. These cases are

1. radiation from a flexible, vibrating, flat membrane surrounded by a rigid, infinite plane (baffled piston),

2. radiation from a flexible, vibrating subset of an otherwise rigid sphere.

The flexibility is in both cases embodied by a non-uniformity $v(\mathbf{r}_s)$, the velocity profile at a point $\mathbf{r}_s$ on the membrane, so that the membrane moves according to $v(\mathbf{r}_s)\, e(t)$ where $e(t)$ is a time-dependent excitation. In the case of a harmonic excitation $e(t) = \exp(i\omega t)$, with ω a real frequency, the radiated pressure in the baffled-piston case is given by one of the Rayleigh integrals, making the connection clear with optical diffraction in which the electric field is given by one of the other Rayleigh integrals. The connection

with optical diffraction is less clear for radiation from a spherical subset of a rigid sphere. In that case, the pressure is the solution of the Helmholtz equation with spherical boundary conditions and assumes the form of an infinite series involving spherical harmonics and spherical Hankel functions with coefficients determined by the boundary conditions.

In this section, we consider the important instances of problem 1 and 2 where the membrane is a circular set and a spherical cap for the respective problems. In these cases, it makes sense to represent the velocity profile as a series involving the Zernike terms (appropriately modified in the spherical-cap case). In recent years, this idea has been worked out in considerable detail by Aarts and Janssen, mainly for the case that the velocity profile is radially and axially symmetric, respectively. In the case of baffled-piston radiation, this has led to semi-analytic expressions for a variety of acoustical quantities. Some of these quantities, such as the on-axis pressure and the far-field pressure, follow rather directly from Rayleigh's integral. Other quantities, such as the pressure at the edge of the piston, the reaction force on the piston, the power and directivity in the far field, and the spatial acoustic impulse response, follow upon using King's integral for the pressure and a considerable amount of advanced calculus. For both the far-field and the quantities associated with King's integral, the basic result of the classical Nijboer-Zernike theory is crucial, since it gives the contribution to the considered quantity of the separate Zernike terms that are used in the expansion of v. The semi-analytic results for the on-axis pressure and the spatial acoustic impulse response have led to the formulation and solution of several inverse problems in which an (unknown) velocity profile is estimated, in terms of expansion coefficients, from measured data in the field. For the case of radiation from a spherical cap with an axially symmetric velocity profile v, the use of orthogonal functions on the cap (rather than on the whole sphere) is crucial in the interest of a stable solution of the inverse problem of estimating v from measured data in the field. The transition from cap expansion coefficients of v to whole-sphere coefficients of v (the latter being required in the series solution of the Helmholtz equation) is provided by the scaling theory for Zernike terms as discussed in Sec. 7.2.

9.2 Baffled-piston radiation

9.2.1 Rayleigh integral and King integral

For circular, baffled-piston radiation, with the piston set S a disk of radius a in the $x-y$ plane and a (non-uniform) velocity profile $v(\mathbf{r}_s)$, $\mathbf{r}_s = (x_s, y_s, 0)$, vanishing for $|\mathbf{r}_s| > a$, the pressure $p(\mathbf{r}, t)$ at a field point $\mathbf{r} = (x, y, z)$ with $z > 0$ due to a harmonic excitation is given by the Rayleigh-II integral

$$p(\mathbf{r}, t) = \frac{i\,\rho_0\,ck}{2\pi}\,e^{i\omega t}\int\limits_S v(\mathbf{r}_s)\,\frac{e^{-ikr'}}{r'}\,dS\ . \tag{62}$$

Here ρ_0 is the density of the medium, c is the speed of sound in the medium, and $k = \omega/c$ is the wave number. Furthermore, t is time and $r' = |\mathbf{r} - \mathbf{r}_s|$ is the distance

between the field point $\mathbf{r}$ and the piston point $\mathbf{r}_s$. The time variable t in $p(\mathbf{r}, t)$ and the harmonic factor $\exp(i\omega t)$ in front of the integral in (62) are omitted in the sequel.

In optical diffraction theory of focused fields, the electric field is given by the Rayleigh-I integral, see [B1], Sec. 2 and in particular Subsec 2.3, which is an integral of a similar type as the one in (62) for the pressure p. Focusing is embodied here by including in the non-uniformity a focal factor $\exp(i\Phi)$, and has the effect that the integral only has to be considered in a small region (the focal volume) when the wavelength of the coherent light source is sufficiently high. Therefore, approximations can be made in the optical setting, leading to the Debye approximation, see [B1], Subsec. 2.2. In the acoustical setting, where no focusing is used normally and where the frequencies of the applied excitations are much smaller, such approximations are not valid. In [B1], Subsec. 2.4 and [J16], Sec. 6, a comparison of the Rayleigh integral and the Debye integral is made in the optical context when the used wavelength λ is varied from small to large.

There is, along with the Rayleigh integral, the King integral

$$p(\mathbf{r}) = i\,\rho_0\,ck \int_0^\infty \frac{e^{-z(u^2-k^2)^{1/2}}}{(u^2-k^2)^{1/2}}\,J_0(wu)\,V(u)\,u\,du \tag{63}$$

for the complex amplitude $p(\mathbf{r})$ of the pressure. Here $w = (x^2+y^2)^{1/2}$ is the distance of the field point $\mathbf{r} = (x, y, z)$ from the axis and

$$V(u) = \int_0^a J_0(u\sigma)\,v(\sigma)\,\sigma\,d\sigma\ , \qquad u \geq 0\ , \tag{64}$$

is the Hankel transform of $v(\mathbf{r}_s)$, $|\mathbf{r}_s| = \sigma$.

9.2.2 Zernike expansion of the velocity profile

The radially symmetric velocity profile $v(\sigma)$, with $\sigma = (x_s^2 + y_s^2)^{1/2}$, is expanded as

$$v(\sigma) = V_s \sum_{l=0}^{\infty} u_l\,R_{2l}^0(\sigma/a)\ , \qquad 0 \leq \sigma \leq a\ , \tag{65}$$

in which V_s is the average velocity so that $u_0 = 1$. The Hankel transform of v, which is the Fourier transform of $v(x_s, y_s)$ considered as a radially symmetric function, follows from the basic result of the Nijboer-Zernike theory as

$$V(u) = a^2\,V_s \sum_{l=0}^{\infty} u_l(-1)^l\,\frac{J_{2l+1}(ua)}{ua}\ , \qquad u \geq 0\ . \tag{66}$$

9.2.3 On-axis and far-field pressure

In [ANZ1], the Rayleigh integral and an explicit result for the Zernike expansion of $\exp(-ikr')/r'$ when $\mathbf{r} = (0, 0, z)$ is an on-axis field point have been used to show that

$$p(\mathbf{r} = (0, 0, z)) = \frac{1}{2}\,\rho_0\, c\, V_s (ka)^2 \sum_{l=0}^{\infty} u_l (-1)^l\, \gamma_l(z, k) \tag{67}$$

in which γ_l is expressed explicitly in terms of spherical Bessel and Hankel functions. Also in [ANZ1], it has been shown by using the Rayleigh integral for large values of $|\mathbf{r}|$ that

$$\begin{aligned} & p(\mathbf{r} = (r\sin\vartheta, 0, r\cos\vartheta)) \;\approx \\ & \approx\; i\,\rho_0\, c\, V_s\, \frac{e^{-ikr}}{r}\, a^2 \sum_{l=0}^{\infty} u_l (-1)^l\, \frac{J_{2l+1}(ka\sin\vartheta)}{ka\sin\vartheta}\ . \end{aligned} \tag{68}$$

The result in (67) is used in [ANZ1] to devise a procedure for estimating an unknown velocity profile v, on the level of Zernike expansion coefficients, from measured on-axis pressures. These coefficients can then be substituted into (68), and this yields an estimate of the far-field. The on-axis data can be collected in the near-field of the radiator and this gives a method for predicting the far-field without having to use an anechoic room.

9.2.4 Edge pressure, reaction force, and power and directivity

In [ANZ2], the King integral (63) and the series expansion (66) have been used to obtain semi-analytic expressions for the pressure at the edge of the piston, the reaction force on the piston, and the power and directivity. For example, the total reaction force

$$F = \int_S p\, dS \tag{69}$$

is expressed as

$$F = 2\pi i\, \rho_0\, kc\, V_s\, a^2 \sum_{l=0}^{\infty} u_l (-1)^l\, I_l(ka) \tag{70}$$

in which $I_l(ka)$ are integrals involving the product of two Bessel function for which in [ANZ2] there are developed explicit power series expansions in ka.

9.2.5 Spatial acoustic impulse responses

The complex amplitude $p(r\,;\,\omega)$ of the pressure is for each wave number $k = \omega/c$ given by the Rayleigh integral (62). In acoustics, the media may be considered to be non-dispersive, and so (62) does not need to be corrected for refractive effects. The velocity potential $\varphi(\mathbf{r}\,;\,\omega)$ is given by

$$\varphi(\mathbf{r}\,;\,\omega) = \frac{1}{i\,\rho_0\, ck}\, p(\mathbf{r}\,;\,\omega)\ , \tag{71}$$

and can be used, via an inverse Fourier transformation with respect to ω, to compute the spatial acoustic impulse response $h(t\,;\,\mathbf{r})$, This impulse response is the potential at time $t > 0$ and field point $\mathbf{r}$ due to a unit instantaneous volume displacement at $t = 0$ of the piston. It turns out that $h(t\,;\,\mathbf{r})$ can be expressed as an integral of the velocity profile v along the arc in the piston plane of piston points that are all at a common distance ct from the field point. In the case that $\mathbf{r} = (0, 0, z)$ is an on-axis point, this arc is non-existing or misses the piston when $ct < z$ or $ct > (z^2 + a^2)^{1/2}$, and when $z \le ct \le (z^2 + a^2)^{1/2}$, one simply has

$$h(t\,;\,(0,0,z)) = cv(R(t\,;\,z))\ , \tag{72}$$

where $R(t\,;\,z) = (c^2t^2 - z^2)^{1/2}$ is the radius of the circle of all points having distance ct to $(0, 0, z)$. This formula (72), giving the velocity profile at any axial point $(0, 0, z)$ in time-warped form, has been used as the basis of an approach to estimate an unknown, radially symmetric velocity profile from measured on-axis impulse response data in [ANZ8].

Using the Zernike expansion (65) of v, integrals $T^0_{2l}(t\,;\,r)$ of Zernike terms along the above-mentioned arcs arise. These integrals can be evaluated, see [ANZ9], in finite terms by using $R^0_{2l}(\rho) = P_l(2\rho^2-1)$ together with the addition theorem for the Legendre polynomials P_l. Thus, there results an expression for $h(t\,;\,\mathbf{r})$ involving the expansion coefficients u_l and the finite-terms expression T^0_{2l}. Also this formula can be used to estimate unknown velocity profiles, now again in terms of expansion coefficients, from measured impulse response data collected in the whole half space in front of the baffle.

9.3 Sound radiation from a flexible cap on a rigid sphere

In [ANZ6], the problem of sound radiation from a spherical cap, with axially symmetric velocity profile on the cap, on a rigid sphere is considered. Due to axial symmetry, the series solution of the Helmholtz equation contains now only Legendre polynomials (= Legendre functions of order 0). Thus, employing spherical coordinates, the complex amplitude of the pressure due to the harmonic excitation $\exp(i\omega t)$, $k = \omega/c$, is given by

$$p(r, \vartheta, \varphi) = -i\,\rho_0\,c\,\sum_{n=0}^{\infty} W_n\,P_n(\cos\vartheta)\,\frac{h_n^{(2)}(kr)}{h_n^{(2)'}(kR)} \tag{73}$$

in which R is the radius of the sphere, and W_n are the expansion coefficients in $W(\vartheta) = \sum_{n=0}^{\infty} W_n\,P_n(\cos\vartheta)$, where

$$W(\vartheta = V(\vartheta)\cos\vartheta\ , \qquad 0 \le \vartheta \le \vartheta_0\ , \tag{74}$$

is the normal component of a velocity profile $V(\vartheta)$ on the cap with aperture angle ϑ_0.

The interest in [ANZ6] is both in forward computation according to (73) and for solving the inverse problem of estimating W in terms of expansion coefficients from measured pressure data around the sphere. However, the representation of W using the expansion coefficients W_n is very inefficient: when W or V is constant on the cap

and 0 outside the cap, the W_n decay as slow as $1/\sqrt{n}$. In [ANZ6], the more efficient representation

$$W(2\arcsin(s_0\rho)) = w_0 \sum_{l=0}^{\infty} u_l \, R_{2l}^0(\rho) \ , \qquad 0 \le \rho \le 1 \ , \tag{75}$$

with $s_0 = \sin\frac{1}{2}\vartheta_0$ (and $u_0 = 1$, as earlier) is proposed. Using the scaling result of [J10], also see Sec. 7.2, it is shown in [ANZ6] that both the W_n required in (73) and the pressure p can be expressed semi-analytically in terms of the u_l and certain explicitly given functions indexed by l.

In [ANZ6], the sound radiation from a true loudspeaker is compared with that from a flexible cap in a rigid sphere on the level of polar plots of the modulus of the pressure. This comparison is continued in [ANZ7] where a variety of other acoustical quantities is considered (baffle-step response, sound power and directivity, acoustic center). The attention in [ANZ7] is limited to forward calculation, and mainly to the cases that W or V is constant in (74). Then the W_n used in (73) assume an explicit form and (73) can be used directly (i.e., without intervention of the u_l in (75)). In general, one can say that the sound radiation from a true loudspeaker can be very well compared with that of a spherical cap on a sphere when cap area and sphere volume are chosen to be equal to membrane area and box volume of the loudspeaker.

10 Computer codes

Some computer codes (MatLab-based) have been made available on the ENZ-webpage.

References

[1] M. Born and E. Wolf, *Principles of Optics* (4th rev. ed., Pergamon Press, New York, 1970).

[2] J.C. Wyant and K. Creath, *Basic wavefront aberration theory for optical metrology*, Chapter I in "Applied optics and optical engineering" (Academic Press, New York, 1992). See also: Jim Wyant, Zernike polynomials

[3] E. Wolf, Y. Li, "Conditions for the validity of the Debye integral representation of focused fields," Opt. Commun. 39 (1981), pp.205-210.

[4] V.N. Mahajan, "Zernike annular polynomials for imaging systems with annular pupils," J. Opt. Soc. Am. 71 (1981), pp. 75-85.

11 ENZ-publications

Journal papers

J1.
A.J.E.M. Janssen, "Extended Nijboer-Zernike approach for the computation of optical point-spread functions," J. Opt. Soc. Am. A 19 (2002), pp. 849-857.
J2.
J.J.M. Braat, P. Dirksen, A.J.E.M. Janssen, "Assessment of an extended Nijboer-Zernike approach for the computation of optical point-spread functions," J. Opt. Soc. Am. A 19 (2002), pp. 858-870.
J3.
P. Dirksen, J.J.M. Braat, A.J.E.M. Janssen, C.A.H. Juffermans, "Aberration retrieval using the extended Nijboer-Zernike approach," Journal of Microlithography, Microfabrication, and Microsystems 2 (2003), pp. 61-68.
J4.
J.J.M. Braat, P. Dirksen, A.J.E.M. Janssen, A. van de Nes, "Extended Nijboer-Zernike representation of the field in the focal region of an aberrated high-aperture optical system," J. Opt. Soc. Am. A 20 (2003), pp. 2281-2292; also in Virtual Journal of Biological Physics Research 6 (2003), issue 12.
J5.
A.J.E.M. Janssen, J.J.M. Braat, P. Dirksen, "On the computation of the Nijboer-Zernike aberration integrals at arbitrary defocus," J. Mod. Opt. 51 (2004), pp. 687-703.
J6.
C. van der Avoort, J.J.M. Braat, P. Dirksen, A.J.E.M. Janssen, "Aberration retrieval from the intensity point-spread function in the focal region using the extended Nijboer-Zernike approach," J. Mod. Opt. 52 (2005), pp. 1695-1728.
J7.
J.J.M. Braat, P. Dirksen, A.J.E.M. Janssen, S. van Haver, A.S. van de Nes, "Extended Nijboer-Zernike approach to aberration and birefringence retrieval in a high-numerical-aperture optical system," J. Opt. Soc. Am. A 22 (2005), pp. 2635-2650.
J8.
P. Dirksen, J.J.M. Braat, A.J.E.M. Janssen, "Estimating resist parameters using the Extended Nijboer-Zernike theory," Journal of Microlithography, Microfabrication, and Microsystems 5 (2006), 013005, pp. 1-11.
J9.
S. van Haver, J.J.M. Braat, P. Dirksen, A.J.E.M. Janssen, "High-NA aberration retrieval with the Extended Nijboer-Zernike vector diffraction theory," J. Eur. Opt. Soc. Rapid Publ. 1 (2006), 06004, pp. 1-8.
J10.
A.J.E.M. Janssen, P. Dirksen, "Concise formula for the Zernike coefficients of scaled pupils," Journal of Microlithography, Microfabrication, and Microsystems 5 (2006), 030501, pp. 1-3.

J11.
A.J.E.M. Janssen, S. van Haver, J.J.M. Braat, P. Dirksen, "Strehl ratio and optimum focus of high-numerical-aperture beams," J. Eur. Opt. Soc. Rapid Publ. 2 (2007), 07008, pp. 1-9.
J12.
S. van Haver, J.J.M. Braat, P. Dirksen, A.J.E.M. Janssen, "High-NA aberration retrieval with the Extended Nijboer-Zernike vector diffraction theory: Erratum," J. Eur. Opt. Soc. Rapid Publ. 2 (2007), 07011e, p. 1.
J13.
A.J.E.M. Janssen, P. Dirksen, "Computing Zernike polynomials of arbitrary degree using the discrete Fourier transform," J. Eur. Opt. Soc. Rapid Publ. 2 (2007), 07012, pp. 1-3.
J14.
J.J.M. Braat, S. van Haver, A.J.E.M. Janssen, P. Dirksen, "Energy and momentum flux in a high-numerical-aperture beam using the extended Nijboer-Zernike diffraction formalism," J. Eur. Opt. Soc. Rapid Publ. 2 (2007), 07032, pp. 1-13.
J15.
A.J.E.M. Janssen, S. van Haver, P. Dirksen, J.J.M. Braat, "Zernike representation and Strehl ratio of optical systems with variable numerical aperture," J. Mod. Opt. 55 (2008), pp. 1127-1157.
J16.
R.M. Aarts, J.J.M. Braat, P. Dirksen, S. van Haver, C. van Heesch, A.J.E.M. Janssen, "Analytic expressions and approximations for the on-axis, aberration-free Rayleigh and Debye integral in the case of focusing fields on a circular aperture," J. Eur. Opt. Soc. Rapid Publ. 3 (2008), 08039, pp. 1-10.
J17.
S. van Haver, J.J.M. Braat, A.J.E.M. Janssen, O.T.A. Janssen, S.F. Pereira, "Vectorial aerial-image computations of three-dimensional objects based on the extended Nijboer-Zernike theory," J. Opt. Soc. Am. A 26 (2009), pp. 1221-1234.
J18.
J.J.M. Braat, S. van Haver, A.J.E.M. Janssen, S.F. Pereira, "Image formation in a multilayer using the Extended Nijboer-Zernike theory," J. Eur. Opt. Soc. Rapid Publ. 4 (2009), 09048, pp. 1-12.
J19.
H.P. Urbach, O.T.A. Janssen, S. van Haver, A.J.H. Wachters, "On the modeling of optical systems containing elements of different scales," J. Mod. Opt. iFirst (2010), pp. 1-13.
J20.
A.J.E.M. Janssen, "New analytic results for the Zernike circle polynomials from a basic result in the Nijboer-Zernike diffraction theory," J. Eur. Opt. Soc. Rapid Publ. 6 (2011), 11028, pp. 1-14.
J21.
A.J.E.M. Janssen, "Computation of Hopkins' 3-circle integrals using Zernike expansions," J. Eur. Opt. Soc. Rapid Publ. 6 (2011), 11059, pp. 1-6.

J22.
J.J.M. Braat, A.J.E.M. Janssen, "Double Zernike expansion of the optical aberration function from its power series expansion," J. Opt. Soc. Am. A 30 (2013), pp. 1213-1222.
J23.
S. van Haver, A.J.E.M. Janssen, "Advanced analytic treatment and efficient computation of the diffraction integrals in the Extended Nijboer-Zernike theory," J. Eur. Opt. Soc. Rapid Publ. 8 (2013), 13044, pp. 1-29.
J24.
A.P. Konijnenberg, L. Wei, N. Kumar, L. Couto Correa Pinto Filho, L. Cisotto, S.F. Pereira, H.P. Urbach, "Demonstration of an optimised focal field with long focal depth and high transmission obtained with the Extended Nijboer-Zernike theory," Opt. Express 22 (2014), pp. 311-324.
J25.
A.J.E.M. Janssen, "Zernike expansion of derivatives and Laplacians of the Zernike circle polynomials," J. Opt. Soc. Am. A 31 (2014), pp. 1604-1613.
J26.
S. van Haver, A.J.E.M. Janssen, "Truncation of the series expressions in the advanced ENZ-theory of diffraction integrals," J. Eur. Opt. Soc. Rapid Publ. 9 (2014), 14042, pp. 1-13.
J27.
J.J.M. Braat, A.J.E.M. Janssen, "Derivation of various transfer functions of ideal or aberrated imaging systems from the three-dimensional transfer function," J. Opt. Soc. Am. A 32 (2015), pp. 1146-1159.

Book chapters

B1.
1. J.J.M. Braat, S. van Haver, A.J.E.M. Janssen, P. Dirksen, "Assessment of optical systems by means of point-spread functions," in Progress in Optics, Vol. 51, E. Wolf, ed., (Elsevier, Amsterdam, The Netherlands, 2008), pp. 349-468.

Ph.D. Dissertations

D1.
A.S. van de Nes, "Rigorous Electromagnetic Field Calculations for Advanced Optical Systems," Ph. D. Dissertation Delft University of Technology (2005), pp. 1-164.
D2.
S. van Haver, "The Extended Nijboer-Zernike diffraction theory and its applications," Ph. D. Dissertation Delft University of Technology (2010), pp. 1-176.

Master thesis

T1.
S. van Haver, "Extended Nijboer-Zernike diffraction and aberration retrieval theory for high-numerical-aperture optical imaging systems," January 2005.

Conference Proceedings

C1.
P. Dirksen, J.J.M. Braat, P. De Bisschop, A.J.E.M. Janssen, C.A.H. Juffermans, Alvina Williams, "Characterization of a projection lens using the extended Nijboer-Zernike approach," Proc. SPIE 4691, Santa Clara, March 2002, pp. 1392-1399.
C2.
P. Dirksen, J. Braat, A.J.E.M. Janssen, C. Juffermans, A. Leeuwestein, "Experimental determination of lens aberrations from the intensity point-spread function in the focal region," Proc. SPIE 5040, Santa Clara, February 2003, pp. 1-10.
C3.
P. Dirksen, J. Braat, A.J.E.M. Janssen, A. Leeuwestein, H. Kwinten, D. Van Steenwinckel, "Determination of resist parameters using the extended Nijboer-Zernike theory," Proc. SPIE 5377, Santa Clara, February 2004, pp. 150-159.
C4.
P. Dirksen, J.J.M. Braat, A.J.E.M. Janssen, A. Leeuwestein, "Aberration retrieval for high-NA optical systems using the extended Nijboer-Zernike theory," Proc. SPIE 5754, San Jose, USA, February-March 2005, pp. 262-273.
C5.
J.J.M. Braat, P. Dirksen, A.J.E.M. Janssen, "Through-focus point-spread function evaluation for lens metrology using the extended Nijboer-Zernike theory," in Fringe 2005 (W. Osten, ed.), Springer, Berlin, 2005, pp. 299-307.
C6.
P. Dirksen, J.J.M. Braat, A.J.E.M. Janssen, A. Leeuwestein, T. Matsuyama, T. Noda, "Aerial image based lens metrology for wafer steppers," Proc. SPIE 6154, San Jose, February 2006, 61540X, pp. 1-11.
C7.
S. van Haver, A.J.E.M. Janssen, P. Dirksen, J.J.M. Braat, "Extended Nijboer-Zernike (ENZ) based evaluation of amplitude and phase aberrations on scaled and annular pupils," meeting digest EOS Advanced Imaging Techniques 2007, Lille, September 12-14, 2007.
C8.
O.T.A. Janssen, S. van Haver, A.J.E.M. Janssen, J.J.M. Braat, H.P. Urbach, S.F. Pereira, "Extended Nijboer-Zernike (ENZ) based mask imaging: efficient coupling of electromagnetic field solvers and the ENZ imaging algorithm," Proc. SPIE 6924, San Jose, February 2008, 692410, pp. 1-9.
C9.
S. van Haver, O.T.A. Janssen, A.J.E.M. Janssen, J.J.M. Braat, H.P. Urbach, S.F. Pereira, "General imaging of advanced 3D mask objects based on the fully-vectorial extended Nijboer-Zernike (ENZ) theory," Proc. SPIE 6924, San Jose, February 2008,

69240U, pp. 1-8.

Presentations at scientific meetings

P1.
P. Dirksen, J.J.M. Braat, P. De Bisschop, A.J.E.M. Janssen, C.A.H. Juffermans, A. Leeuwestein, "Characterization of a projection lens using the extended Nijboer-Zernike approach", SPIE conference on Microlithography, Santa Clara, March 3-8, 2002.
P2.
J.J.M. Braat, P. Dirksen, A.J.E.M. Janssen, A. van de Nes, "Extended Nijboer-Zernike representation of the field in the focal region of an aberrated high-aperture optical system, poster presented at the Annual Meeting of OSA, Orlando, October 2002.
P3.
P. Dirksen, J.J.M. Braat, A.J.E.M. Janssen, C. Juffermans, A. Leeuwestein, "Experimental determination of lens aberrations from the intensity point-spread function in the focal region," SPIE conference on Microlithography, February 23-28, 2003.
P4.
J.J.M. Braat, P. Dirksen, A.J.E.M. Janssen, A.S. van de Nes, "Extended Nijboer-Zernike description of the high-aperture focal field created by a beam with angular momentum", presented at Focus on Microscopy 2003, Genova, April 13-16, 2003.
P5.
P. Dirksen, J.J.M. Braat, A.J.E.M. Janssen, A. Leeuwestein, H. Kwinten, D. van Steenwinckel, "Determination of resist parameters using the extended Nijboer-Zernike theory," SPIE conference on Microlithography, February 21-26, 2004.
P6.
J.J.M. Braat, P. Dirksen, A.J.E.M. Janssen, A.S. van de Nes, "Quality assessment of focusing optics by aberration retrieval using the extended Nijboer-Zernike diffraction theory", presented at Focus on Microscopy 2004, Philadelphia, April 4-7, 2004.

P7.
P. Dirksen, J.J.M. Braat, A.J.E.M. Janssen, D. van Steenwinckel, A. Leeuwestein, "Aberration retrieval for a lithographic lens in the presence of focus variation and spatial diffusion," IISB Lithography Simulation Workshop, Hersbruck, Germany, September 17-19, 2004.
P8.
J.J.M. Braat, P. Dirksen, A.J.E.M. Janssen, "Extended Nijboer-Zernike analysis for vectorial diffraction calculations and aberration retrieval," IISB Lithography Simulation Workshop, Hersbruck, Germany, September 17-19, 2004.
P9.
J.J.M. Braat, P. Dirksen, A.J.E.M. Janssen, A.S. van de Nes, "Complex pupil function reconstruction using the extended Nijboer-Zernike diffraction theory," abstract presented at OSA Annual Meeting, October 2004, Rochester, USA; corresponding poster presentation: "Complex pupil function reconstruction at high numerical aperture using

the extended Nijboer-Zernike diffraction theory".

P10.

P. Dirksen, J.J.M. Braat, A.J.E.M. Janssen, A. Leeuwestein, "Aberration retrieval for high-NA optical systems using the Extended Nijboer-Zernike theory," SPIE conference on Microlithography, San Jose, February 27 - March 4, 2005.

P11.

J.J.M. Braat, P. Dirksen, A.J.E.M. Janssen, A. van de Nes, "Polarisation-aberration retrieval for high-NA systems using the extended Nijboer-Zernike diffraction theory", presented at Focus on Microscopy 2005, Jena, March 20-24, 2005.

P12.

J.J.M. Braat, P. Dirksen, A.J.E.M. Janssen, "Through-focus point-spread function evaluation for lens metrology using the Extended Nijboer-Zernike theory", presented at Fringe 2005, Stuttgart, September 12-14, 2005.

P13.

J.J.M. Braat, P. Dirksen, A.J.E.M. Janssen, A. Leeuwestein, T. Matsuyama, T. Noda, "Aerial image based lens metrology for wafer steppers," SPIE conference on Microlithography, San Jose, February 19-24, 2006.

P14.

S. van Haver, J.J.M. Braat, P. Dirksen, A.J.E.M. Janssen, "High-NA lens characterization by through-focus intensity measurements," presented at EOS Annual Meeting 2006, Paris, October 16-19, 2006.

P15.

S. van Haver, A.J.E.M. Janssen, P. Dirksen, J.J.M. Braat, "Extended Nijboer-Zernike (ENZ) based evaluation of amplitude and phase aberrations on scaled and annular pupils," to be presented at Advanced Imaging Techniques 2007, Lille, September 12-14, 2007.

P16.

S. van Haver, A.J.E.M. Janssen, P. Dirksen, J.J.M. Braat, "Imaging based on the Extended Nijboer-Zernike (ENZ) formalism," presented at EOS Advanced Imaging Techniques 2007, Lille, September 12-14, 2007.

P17.

S. van Haver, O.T.A. Janssen, A.M. Nugrowati, J.J.M. Braat, S.F. Pereira, "Novel approach to mask imaging based on the Extended Nijboer-Zernike (ENZ) diffraction theory," poster presented at MNE'07, Copenhagen, September 23-26, 2007. (Received 1st price in best poster award.)

P18.

O.T.A. Janssen, S. van Haver, A.J.E.M. Janssen, J.J.M. Braat, H.P. Urbach, S.F. Pereira, "Extended Nijboer-Zernike (ENZ) based mask imaging: efficient coupling of electromagnetic field solvers and the ENZ imaging algorithm," presented at SPIE conference on Microlithography, San Jose, February 2008.

P19.

S. van Haver, O.T.A. Janssen, A.J.E.M. Janssen, J.J.M. Braat, H.P. Urbach, S.F. Pereira, "General imaging of advanced 3D mask objects based on the fully-vectorial extended Nijboer-Zernike (ENZ) theory," presented at SPIE conference on Microlithog-

raphy, San Jose, February 2008.

P20.

S. van Haver, O.T.A. Janssen, A.M. Nugrowati, J.J.M. Braat, S.F. Pereira, "Combining various optical simulation tools to enable complex optical system simulations," poster presented at NEMO meeting, Santiago de Compostela, Spain, July, 2008.

P21.

S. van Haver, O.T.A. Janssen, A.J.E.M. Janssen, J.J.M. Braat, S.F. Pereira, P. Evanschitzky, "Characterization of a novel mask imaging algorithm based on the Extended Nijboer-Zernike (ENZ) formalism," poster presented at MNE conference, Athens, Greece, September, 2008.

P22.

S. van Haver, O.T.A. Janssen, J.J.M. Braat, S.F. Pereira, "An alternative method for advanced lithographic imaging: the Extended Nijboer-Zernike formalism," lecture at 6th Fraunhofer IISB Lithography Simulation Workshop, Athens, Greece, September, 2008.

P23.

S. van Haver, O.T.A. Janssen, A.J.E.M. Janssen, J.J.M. Braat, S.F. Pereira, "Image simulations of extended objects using an algorithm based on the Extended Nijboer-Zernike (ENZ) formalism," poster presented at the EOS Annual Meeting 2008, Paris, 29 September - 3 October, 2008. (Received 1st price in best poster award.)

P24.

S. van Haver, A.J.E.M. Janssen, J.J.M. Braat, S.F. Pereira, "Evaluation of scaled and annular pupils within the frame-work of the Extended Nijboer-Zernike (ENZ) formalism," poster presented at the OSA FiO 2008, Rochester NY, 19 October - 23 October, 2008.

P25.

S. van Haver, O.T.A. Janssen, J.J.M. Braat, S.F. Pereira, "Characterization of a novel mask imaging algorithm based on the Extended Nijboer-Zernike (ENZ) formalism," poster presented at Micro-Nano Conference, Wageningen, The Netherlands, November, 2008. (Same poster as presented at MNE 2008, see item 21.)

P26.

S. van Haver, A.J.E.M. Janssen, P. Dirksen, J.J.M. Braat, "Extended Nijboer-Zernike based imaging into an image region containing a layered configuration," presented at EOS Advanced Imaging Techniques 2009, Jena, Germany, June 10-12, 2009.

P27.

J.J.M. Braat, S. van Haver, S.F. Pereira, "Microlens quality assessment using the Extended Nijboer-Zernike (ENZ) diffraction theory," presented at EOS Optical Microsystems 2009, Capri, Italy, September 27-30, 2009.

P28.

S. van Haver, J.J.M. Braat, S.F. Pereira, "Accurate and efficient simulation of resist images generated by advanced lithographic systems using the Extended Nijboer-Zernike (ENZ) diffraction theory," presented at Micro-Nano Conference, Delft, The Netherlands, November, 2009.

P29.

J.J.M. Braat, "Extended Nijboer-Zernike diffraction theory," presented at SPAM-Winterschool, Delft, The Netherlands, January 2011.

arXiv publications

arXiv1.
A.J.E.M. Janssen, "Zernike circle polynomials and infinite integrals involving the product of Bessel functions," arXiv:1007.0667v1 [math-ph] 5 Jul 2010, pp. 1-45.
arXiv2.
A.J.E.M. Janssen, "A generalization of the Zernike circle polynomials for forward and inverse problems in diffraction theory," arXiv:1110.2369v1 [math-ph] 11 Oct 2011, pp. 1-43.
arXiv3.
A.J.E.M. Janssen, "Zernike expansions of derivatives and Laplacians of the Zernike circle polynomials," arXiv:1404.1766v1 [math-ph] 7 Apr 2014, pp. 1-31.
arXiv4.
S. van Haver, A.J.E.M. Janssen, "Truncation strategy for the series expressions in the advanced ENZ-theory of diffraction integrals," arXiv:1407.6589v1 [physics.comp-ph] 24 Jul 2014, pp. 1-54.

ANZ publications (journal papers and conference proceedings)

ANZ1.
R.M. Aarts, A.J.E.M. Janssen, "On-axis and far-field sound radiation from resilient flat and dome-shaped radiators," J. Acoust. Soc. Am. 125 (2009), pp. 1444–1455.
ANZ2.
R.M. Aarts, A.J.E.M. Janssen, "Sound radiation quantities arising from a resilient circular radiator," J. Acoust. Soc. Am. 126 (2009), pp. 1776–1787.
ANZ3.
R.M. Aarts, A.J.E.M. Janssen, "Estimating the velocity profile and acoustical quantities of a harmonically vibrating membrane from on-axis pressure data," presented at NAG/DAGA 2009 Conference, Rotterdam, March 2009.
ANZ4.
R.M. Aarts, A.J.E.M. Janssen, "Estimating the velocity profile and acoustical quantities of a harmonically vibrating loudspeaker membrane from on-axis pressure data," J. Audio Eng. Soc. 57 (2009), pp. 1004–1015.
ANZ5.
R.M. Aarts, A.J.E.M. Janssen, "Authors' reply to comments on "Estimating the velocity profile and acoustical quantities of a harmonically vibrating loudspeaker membrane from on-axis pressure data"," J. Audio Eng. Soc. 58 (2010), pp. 308–310.
ANZ6.
R.M. Aarts, A.J.E.M. Janssen, "Sound radiation from a resilient spherical cap on a rigid sphere," J. Acoust. Soc. Am. 127 (2010), pp. 2262–2273.
ANZ7.
R.M. Aarts, A.J.E.M. Janssen, "Modeling a loudspeaker as a flexible cap on a rigid sphere," presented at AES 128$^{\text{th}}$ Convention, London, May 2010.
ANZ8.
R.M. Aarts, A.J.E.M. Janssen, "Acoustic holography for piston sound radiation with non-uniform velocity profiles," presented at ICSV 17, Cairo, July 2010.
ANZ9.
R.M. Aarts, A.J.E.M. Janssen, "Spatial impulse responses from a flexible baffled circular piston," J. Acoust. Soc. Am. 129 (2011), pp. 2952-2959.
ANZ10.
R.M. Aarts, A.J.E.M. Janssen, "Sound radiation of a non-rigid piston and pole cap compared with loudspeakers," presented at NAG 2011 Conference, Utrecht, March 2011.
ANZ11.
R.M. Aarts, A.J.E.M. Janssen, "Comparing sound radiation from a loudspeaker with that from a flexible spherical cap on a rigid sphere," J. Audio Eng. Soc. 59 (2011), pp. 201-212.
ANZ12.
R.M. Aarts, A.J.E.M. Janssen, "Sound radiation from a loudspeaker, from a spherical pole cap, and from a piston in an infinite baffle," Noise&Vibration Worldwide (April 2012), pp. 12-19.

Most references in this text can be found on the Extended Nijboer-Zernike website itself: Extended Nijboer-Zernike (ENZ) Analysis and Aberration Retrieval.